

# MIMIR: Masked Image Modeling for Mutual Information-based Adversarial Robustness

Xiaoyun Xu<sup>1</sup>, Shujian Yu<sup>2</sup>, Zhuoran Liu<sup>1</sup>, Stjepan Picek<sup>1</sup>

<sup>1</sup>Radboud University Nijmegen, The Netherlands

<sup>2</sup>Vrije Universiteit Amsterdam, The Netherlands

{xiaoyun.xu,zhuoran.liu,stjepan.picek}@ru.nl, s.yu3@vu.nl,

## Abstract

Vision Transformers (ViTs) achieve excellent performance in various tasks, but they are also vulnerable to adversarial attacks. Building robust ViTs is highly dependent on dedicated Adversarial Training (AT) strategies. However, current ViTs' adversarial training only employs well-established training approaches from convolutional neural network (CNN) training, where pre-training provides the basis for AT fine-tuning with the additional help of tailored data augmentations. In this paper, we take a closer look at the adversarial robustness of ViTs by providing a novel theoretical Mutual Information (MI) analysis in its autoencoder-based self-supervised pre-training. Specifically, we show that MI between the adversarial example and its latent representation in ViT-based autoencoders should be constrained by utilizing the MI bounds. Based on this finding, we propose a masked autoencoder-based pre-training method, MIMIR, that employs an MI penalty to facilitate the adversarial training of ViTs. Extensive experiments show that MIMIR outperforms state-of-the-art adversarially trained ViTs on benchmark datasets with higher natural and robust accuracy, indicating that ViTs can substantially benefit from exploiting MI. In addition, we consider two adaptive attacks by assuming that the adversary is aware of the MIMIR design, which further verifies the provided robustness. Our code and trained models are publicly available at the anonymous link.<sup>1</sup>

## 1 Introduction

Adversarial training (Madry et al. 2018) is one of the standard techniques to build robust models. Regarding adversarial training for ViTs, early works focus on investigating the unique attention mechanism of ViTs. There, robustness can be improved by randomly dropping gradient according to attention (Mo et al. 2022) or improving training efficiency by dropping low-attention image embeddings (Wu et al. 2022). The majority of recent works focus on improving the ViTs' adversarial training based on experience with CNNs, given AT's success in building robust CNNs. Looking at the adversarial training recipe differences between ViTs and CNNs, *strong data augmentation*, e.g., Randaugment (Cubuk et al. 2020), CutMix (Yun et al. 2019), and MixUp (Zhang et al. 2018), show positive influence in CNN but are ineffective for ViTs AT and sometimes even reduce

the AT performance of ViTs (Bai et al. 2021; Singh, Croce, and Hein 2023). To mitigate this, the distortion magnitudes of Randaugment and the probability of applying MixUp or CutMix need to be progressively increased (Bai et al. 2021). Similar problems of strong data augmentations are also observed by (Debenedetti, Sehwag, and Mittal 2023), where basic data augmentations, i.e., random-resize-and-crop, horizontal-flipping, and color-jitter with high weight decay are shown to be promising to improve ViT adversarial training.

Another common practice in ViT adversarial training is to leverage *pre-trained* models, which has also been extensively explored (Mo et al. 2022; Singh, Croce, and Hein 2023). Fine-tuning on natural pre-trained models could benefit the adversarial robustness of ViTs. For instance, recently, AdvXL (Wang et al. 2024) introduced an efficient and effective adversarial training strategy for giant models on web-scale datasets. However, as the current ViT adversarial training strategies are mainly inherited from CNN AT, the key factor that drives the success of pre-training has not been completely revealed. For instance, pre-training with ImageNet-21K and SimMIM (Xie et al. 2022) performs similarly to the model trained from scratch, and even the CLIP (Radford et al. 2021) pre-trained model shows a performance drop (Liu et al. 2024).

In this work, we aim to provide an in-depth analysis of ViT's robustness using MI, focusing on self-supervised pre-training. Information Bottleneck (IB) has been previously used in supervised learning to analyze adversarial robustness, where a joint objective of simultaneously minimizing the MI between inputs and latent features while maximizing the MI between labels and latent features is introduced to mitigate the impact of the adversarial noise in the inputs. Regarding the task of ViT adversarial training, we provide a novel theoretical analysis for the self-supervised autoencoder, showing that the self-supervised ViT benefits from decreasing the MI between inputs and latent features. Based on this finding, we propose a theoretically grounded adversarial pre-training method, **Masked Image Modeling for Mutual Information-based Adversarial Robustness (MIMIR)**. Figure 1 provides an illustrative diagram of MIMIR.

MIMIR substantially improves the adversarial robustness of ViT models as demonstrated by comprehensive

<sup>1</sup><https://anonymous.4open.science/r/MIMIR-5444>

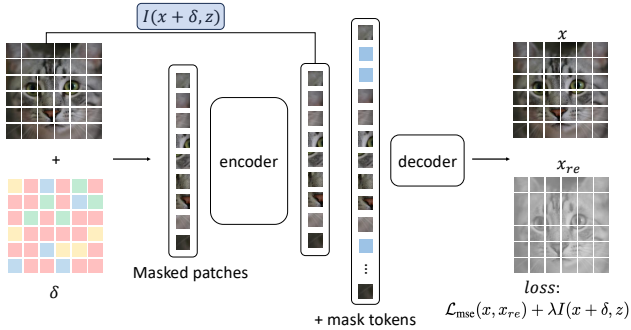


Figure 1: Diagram illustrating the working mechanism of MIMIR. In the pre-training, adversarial perturbations  $\delta$  are generated and added to natural images  $x$  to create adversarial images  $x + \delta$ , as shown on the left. Patches of generated adversarial images are fed as training data to the ViT-based autoencoder, where the output of decoder  $x_{re}$  and the natural input image  $x$  are used to calculate the loss. In particular, we propose using MI ( $I(x + \delta, z)$ ) as an additional penalty to compose the pre-training loss of MIMIR, as shown in the bottom right. After pre-training, a trained encoder is combined with a randomly initialized classification layer as the final model that is further fine-tuned for classification tasks.

experiments on ImageNet-1K (Deng et al. 2009), Tiny-ImageNet (Le and Yang 2015), and CIFAR-10 (Krizhevsky, Hinton et al. 2009). We also provide an experimental comparison with the state-of-the-art, showing the effectiveness of MIMIR in improving both natural and adversarial prediction accuracy (see Section 4.2).

Our main contributions are:

- By revising the current ViT AT strategies, we point out that ViT adversarial pre-training methods compromise natural accuracy and lack systematic analysis. To this end, we provide a theoretical analysis using adversarial examples and the Mutual Information penalty. The MI bounds motivate us to decrease MI between adversarial examples and learned latent representation.
- Based on the findings of our analysis, we propose an efficient self-supervised defense MIMIR against adversarial attacks on ViTs. We systematically evaluate MIMIR using three datasets and multiple model scales under various adversarial attacks, demonstrating its superiority.
- We show MIMIR is resistant to two adaptive attacks, where the adversary is aware of MIMIR design. We build a PGD-fea attack that increases the distance between features extracted from natural and adversarial examples. Moreover, we build a PGD-MI attack that includes the MI penalty as the learning objective to find adversarial examples.

## 2 Background and Related Work

**Adversarial Examples.** Adversarial example (Dalvi et al. 2004; Biggio et al. 2013; Szegedy et al. 2014) refer to applying imperceptible perturbations to the original input of the target machine learning model, which misleads the victim

model. Given an  $L$ -layer transformer network  $F_\theta$  for classification in  $d_Y$ -dimensional space, and a training dataset  $D = \{(x_i, y_i)\}_{i=1}^n$  in  $d_X$ -dimensional space, the adversarial perturbation  $\delta$  is calculated by maximizing:

$$\max_{\delta \in S} \mathcal{L}_{CE}(\theta, x_i + \delta, y_i), \quad (1)$$

The generated adversarial examples are as similar as possible to the original natural examples by limiting  $\delta$  to a relatively small domain:

$$S = B(x_i, r) = \{\delta \in \mathbb{R}^{d_X} : \|\delta\|_\infty \leq r\}, \quad (2)$$

where  $S$  is the  $l_\infty$ -ball of radius  $r$  at a position  $x_i$  in  $\mathbb{R}^{d_X}$ . The distance between  $x_i$  and  $x_i + \delta$  can be evaluated by norms such as  $l_0$ ,  $l_2$ , and  $l_\infty$ .

When using the above adversarial examples to conduct adversarial training, the learning objective is:

$$\min_{\theta} \max_{\delta \in S} \mathcal{L}_{CE}(\theta, x_i + \delta, y_i). \quad (3)$$

**Information Bottleneck (IB).** The IB concepts were first proposed in (Tishby, Pereira, and Bialek 2000) and further developed for deep learning in (Tishby and Zaslavsky 2015; Shwartz-Ziv and Tishby 2017). It has been widely used to improve adversarial robustness (Xu, Perin, and Picek 2023; Alemi et al. 2017; Yu, Yu, and Príncipe 2021; Wang et al. 2021). IB describes the generalization of a deep neural network in two phases: 1) empirical error minimization (ERM) and 2) representation compression. For a network with input  $x$  and label  $y$ , there is an intermediate representation  $t_l$  for each layer  $l$ , i.e., the output of  $l$ -th layer. The IB principle aims to keep more relevant information in  $t_l$  about target  $y$  while decreasing the irrelevant information about input  $x$ . The information between intermediate representation  $t_l$  and input  $x$  or label  $y$  is quantified by MI, denoted by  $I$ .

**Adversarial Robustness of ViTs.** PGD (Madry et al. 2018) adversarial training is considered one of the most effective defenses that can withstand adaptively designed attacks (Athalye, Carlini, and Wagner 2018). Due to the difference between CNNs and ViTs, there have been substantial recent efforts to explore new adversarial training approaches for ViTs. EasyRobust (Mao et al. 2022) evaluates the robustness of ViTs using PGD adversarial training. (Mo et al. 2022; Bai et al. 2021; Debenedetti, Sehwag, and Mittal 2023) demonstrate the classical training recipe for CNN is not suitable for ViTs and present new adversarial training strategies for ViTs by evaluating different hyperparameters and data augmentation policies. (Mo et al. 2022) also finds that pre-training with natural data provides better robustness after adversarial fine-tuning. (Singh, Croce, and Hein 2023) explores the effect of strong pre-training and replacing the patch embedding in ViTs with convolutional blocks. AdvXL (Wang et al. 2024) shows an outstanding performance of giant models and web-scale data with adversarial pre-training and fine-tuning. However, (Liu et al. 2024) provides a different view that pre-training with ImageNet-21K and SimMIM (Xie et al. 2022) performs similarly to the model trained from scratch, and the CLIP pre-trained model has a performance drop. Unlike existing works, we provide a formal and in-depth analysis leveraging MI, based on which we introduce a new adversarial pre-training scheme.

### 3 MIMIR

#### 3.1 Threat Model

**Adversary’s Goal.** The attacker aims to fool the trained model by decreasing the overall classification accuracy (non-targeted) or forcing the model to recognize an input as a specific target (targeted). The image perturbations are limited by the  $l_\infty$  norm for invisibility.

**Adversary Knowledge.** The attacker has white-box access to the model, including training data, architectures, hyper-parameters, and model weights. The attacker can implement iterative attacks and unlimited queries to update adversarial examples multiple times in white and black-box settings. Adversarial examples can be created according to model architectures, parameters, the gradients of loss function, and datasets. The adversary can adaptively design new attacks for a specific model according to the design details of the defense method.

**Defender’s Goal.** The defender’s main goal is to train a robust model against potential adversarial attacks and prevent the performance of natural data from decreasing significantly. In addition, the defense method should be robust against adaptive attacks specifically designed for it.

#### 3.2 Design Intuition

MIM has been proved useful as a pre-training method for ViTs on various tasks (Vincent et al. 2010; He et al. 2022; Wei et al. 2022; Bao et al. 2022). To train a powerful model using MIM, one can mask out a part of the foreground of inputs and reconstruct it using the model. Masking out the foreground instead of the background reduces discriminative information in visible information to the model. Reconstructing foreground parts is harder than background and helps the model learn more discriminative information (Wang et al. 2023). Inspired by this phenomenon, we aim to build a more difficult task by adding adversarial perturbations to natural inputs. The adversarial perturbations increase the distance between the input and reconstruction target. If we can reconstruct natural inputs from adversarial examples, it means the features learned by the model are robust against adversarial attacks. In other words, we want the encoder to learn a latent representation that does not carry information concerning adversarial perturbations while enabling the decoder to reconstruct the natural image. Note that simply masking out all foreground does not make sense, as it would render the reconstruction of meaningful content infeasible. From the perspective of IB, there is a bottleneck between the encoder and decoder. Our adversarial pre-training task contains two information sources: the natural data  $x$  and the adversarial perturbations  $\delta$ . As the information flows through the bottleneck, adversarial information from  $\delta$  is eliminated. The natural information from  $x$  is maintained because of the constraint when reconstructing the target  $x$ .

#### 3.3 Design Details

**Autoencoder.** MIMIR follows the general design of MAE (He et al. 2022), consisting of an encoder  $f_e$  and a decoder  $f_d$ . As with other autoencoders, the encoder extracts

---

#### Algorithm 1: MIMIR Pre-training

---

**Input:** training data  $D$ , number of epochs  $E$ , encoder  $f_e$ , decoder  $f_d$ , network parameters  $\theta$ ,  $\mathcal{L}_{\text{mse}}$ ,  $\lambda$ .  
**Output:** optimized weights  $\theta$

```
1: for  $e = 0 \rightarrow E - 1$  do
2:    $x \leftarrow \text{sample\_batch}(D)$ 
3:    $\delta \leftarrow \text{random\_initialization}$ 
4:    $x_{re} \leftarrow f_d \circ f_e(x + \delta)$ 
5:    $\delta \leftarrow \underset{\delta \in S}{\text{max}} \mathcal{L}_{\text{mse}}(x + \delta, x_{re})$ 
6:   Forward:
7:    $z \leftarrow f_e(x + \delta)$ 
8:    $x_{re} \leftarrow f_d(z)$ 
9:    $\text{loss} \leftarrow \mathcal{L}_{\text{mse}}(x, x_{re}) + \lambda I(x + \delta, z)$ 
10:  Backward:
11:   $\theta \leftarrow \theta - \alpha \nabla \text{loss}$ 
12: end for
```

---

discriminative features  $z$  from inputs  $x$ . The decoder reconstructs original inputs according to the discriminative features. Following ViT (Dosovitskiy et al. 2021), the input  $x$  is separated into non-overlapping image patches. We randomly mask out a part of the patches and use the remaining patches as inputs for the following process in the encoder. This random masking process uses uniform distribution to prevent potential sampling bias, such as all foreground information being masked, as it becomes infeasible to find the reconstruction target. Thus, we aim to keep a part of the foreground as a hint for reconstruction. The information of masked content is recorded as mask tokens  $m$ , not used by the encoder but reserved for later use by the decoder. Each token is a learned vector indicating the presence of a masked patch to be predicted. The mask token is shared by all inputs of the decoder. Like unmasked patches, mask tokens are also assigned corresponding positional embeddings to be in the correct location in the reconstructed image. We emphasize that mask tokens are not used in the encoder part.

To train a ViT, we use the same transformer blocks as ViT to build the encoder. The encoder only processes the visible patches, making training much more efficient. When converting to other architectures, such as ConViT (D’Ascoli et al. 2021), we use corresponding transformer blocks to build the encoder. The decoder accepts the encoded visible image patches and mask tokens as inputs. The decoder is built using the same transformer blocks as the encoder instead of using ViT (Dosovitskiy et al. 2021) transformer blocks for all. Then, the decoder is followed by a fully connected layer, which outputs the same number of patches as the original image.

**Adversarial Pre-training Target.** The training target is to extract discriminative features from visible image patches by the encoder and then reconstruct the invisible patches by the decoder. Therefore, we need a differentiable measurement to quantify the distance between the original image and the reconstructed results. Following the original MAE (He et al. 2022), this distance is measured by Mean Squared Error (MSE). To create a more difficult reconstruction task, we apply adversarial perturbations  $\delta$  on the inputs of the encoder. Thus, the adversarial perturbations are also masked

along with the image upon input into the encoder. The decoder reconstructs the original natural inputs by using the latent features  $z$  extracted from adversarial examples. The outputs of decoder  $x_{re}$  and  $x$  are used to calculate the MSE loss, which is further used to optimize the model. Note that the reconstruction differs from the original MAE; we do not use the encoder inputs as reconstruction targets. Formally, the pre-training process (described in Algorithm 1) can be written as follows:

$$\begin{aligned} z &= f_e(x + \delta), x_{re} = f_d(z), \\ loss_{mse} &= \mathcal{L}_{mse}(x, x_{re}). \end{aligned} \quad (4)$$

**MI as Penalty.** Inspired by IB, we show in Section 3.4 that MI between latent representation and adversarial examples decreases as the accuracy on adversarial examples, i.e.,  $I(x + \delta, z)$  is decreasing while training. Motivated by this finding, we directly use  $I(x + \delta, z)$  as a penalty in our final loss function:

$$loss_{mi} = \mathcal{L}_{mse}(x, x_{re}) + \lambda I(x + \delta, z), \quad (5)$$

where  $\lambda$  is a regularizer for the MI penalty. We use  $I(x + \delta, z)$  instead of  $I(x, z)$  as a penalty. This is because  $x \rightarrow x + \delta \rightarrow z$  follows the Markov chain since  $z$  is extracted from  $x + \delta$ . According to Data Processing Inequality (DPI) (Beaudry and Renner 2011),  $I(x, z) \leq I(x + \delta, z)$ .  $I(x + \delta, z)$  is closer to  $z$  on the Markov chain.

**Generating Adversarial Examples.** To conduct the adversarial pre-training, we need an attack that finds proper adversarial perturbations  $\delta$ . As the autoencoder does not provide classification outputs, it is not possible to directly use existing adversarial attacks, such as PGD (Madry et al. 2018). Nevertheless, it is feasible to design a new algorithm to find  $\delta$  by maximizing  $loss_{mse}$  in Eq. (4). As the feature  $z$  is extracted from only visible image patches, we only attack the visible patches. We do not add any perturbations to mask tokens since the outputs of the autoencoder are only impacted by visible patches. Then, the adversarial pre-training learning objective can be written as:

$$\begin{aligned} \mathcal{L}_{adv} &= \max_{\delta \in S} \mathcal{L}_{mse}(f_d \circ f_e(x + \delta), x), \\ \min_{\theta} \mathcal{L}_{adv} &+ \lambda I(x + \delta, z), \end{aligned} \quad (6)$$

where  $\theta$  are the autoencoder parameters. After the autoencoder is trained, we discard the decoder and initialize a classification layer for the encoder to build a complete model. Finally, the complete model is fine-tuned by AT methods.

### 3.4 Theoretical Justification

Next, we provide theoretical justification showing that the MI between the adversarial example and its latent representation, i.e.,  $I(x + \delta, z)$ , should be constrained. Let  $F$  denote any classifier trained on natural samples with desirable prediction accuracy, which may suffer from adversarial attacks. We begin our analysis by first presenting Lemma 3.1.

**Lemma 3.1.** *Let  $F(x + \delta)$  and  $F(x_{re})$  denote, respectively, the predicted labels of adversarial sample  $x + \delta$  and reconstructed sample  $x_{re}$ , we have:*

$$I(F(x + \delta), F(x_{re})) \leq I(F(x + \delta), x_{re}) \leq I(x + \delta, z). \quad (7)$$

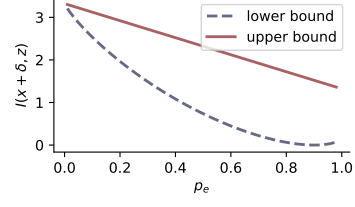


Figure 2: The example plots for the lower and upper bounds on the MI in Propositions 3.2 and 3.3. The entropy ( $H(\cdot)$ ) is chosen uniformly at random from a set of 10 classes. The lower bound reaches its minimum at  $p_e = 0.9$ .

*Proof.* There are two Markov chains:

$$\begin{aligned} x + \delta &\rightarrow F(x + \delta), \\ z &\rightarrow x_{re} \rightarrow F(x_{re}), \end{aligned} \quad (8)$$

which implies that  $F(x + \delta)$  is an indirect observation of  $x + \delta$ , whereas both  $F(x_{re})$  and  $x_{re}$  are indirect observations of  $z$ .

By the data processing inequality (DPI), we have

$$I(x + \delta, z) \geq I(F(x + \delta), z), \quad (9)$$

and

$$I(F(x + \delta), z) \geq I(F(x + \delta), x_{re}) \geq I(F(x + \delta), F(x_{re})). \quad (10)$$

□

Now, we define  $p_e$  as the probability that the predicted label of  $x + \delta$  by  $F$  is not equal to that of  $x_{re}$ , i.e.,  $p_e = \mathbb{P}(F(x + \delta) \neq F(x_{re}))$ . Intuitively, our autoencoder is trained to recover only natural sample  $x$  without any interference from  $\delta$ . Hence, a relatively large value of  $p_e$  is expected. In the following, we establish the connection between  $p_e$  and  $I(x + \delta, z)$  with both lower and upper bounds, showing that minimizing  $I(x + \delta, z)$  also encourages a large value of  $p_e$ .

**Proposition 3.2.** *Let  $H(\cdot)$  denote the information entropy and  $H_b(p_e) = -p_e \log_2 p_e - (1 - p_e) \log_2 (1 - p_e)$  be the binary entropy, we have:*

$$H(F(x + \delta)) - H_b(p_e) - p_e \log(|F(x + \delta)| - 1) \leq I(x + \delta, z), \quad (11)$$

where  $|F(x + \delta)|$  is the total number of categories.<sup>2</sup>

*Proof.* By the chain rule of MI, we have

$$I(F(x + \delta), F(x_{re})) = H(F(x + \delta)) - H(F(x + \delta)|F(x_{re})). \quad (12)$$

By applying Fano's inequality (Fano 1949; Ocal et al. 2019), we obtain:

$$H(F(x + \delta)|F(x_{re})) \leq H_b(p_e) + p_e \log(|F(x + \delta)| - 1). \quad (13)$$

Adding  $I(F(x + \delta), F(x_{re}))$  to both sides of Eq. (13):

$$\begin{aligned} H(F(x + \delta)) - H_b(p_e) - p_e \log(|F(x + \delta)| - 1) \\ \leq I(F(x + \delta), F(x_{re})) \\ \leq I(x + \delta, z). \end{aligned} \quad (14)$$

The last line of Eq. (14) is by Lemma 3.1. □

<sup>2</sup>For instance, for CIFAR-10,  $|F(x + \delta)| = 10$ .

Table 1: Comparison with SOTA results on ImageNet-1K under  $\epsilon = 4/255$ . The robust accuracy refers to accuracy under AutoAttack. The ‘‘Adv. Steps’’ refers to attack steps for generating adversarial examples for AT. †The results of (Wang et al. 2024) are evaluated using 20-step PGD (AutoAttack is designed as a more powerful alternative to PGD). Although it only uses 20 epochs, it costs more time due to huge datasets for pre-training and fine-tuning.

Architecture	Params (M)	FT	FT Epoch	Adv. Steps	Source	Natural	Robust
ResNet-50	25.0	PGD	100	1	(Bai et al. 2021)	67.44	35.54
DeiT-S	22.1	PGD	100	1	(Bai et al. 2021)	66.62	36.56
DeiT-S	22.1	PGD	110	1	(Debenedetti, Schwag, and Mittal 2023)	66.80	37.90
ViT-S	22.1	PGD	120	3	(Mao et al. 2022)	66.43	39.20
ViT-S	22.1	PGD	300	3	(Liu et al. 2024)	70.7	43.7
RobArch-S	26.1	PGD	110	3	(Peng et al. 2023)	70.17	44.14
ViT-S	22.1	APGD	300	2	(Singh, Croce, and Hein 2023)	69.22	44.04
ViT-S	22.1	APGD	300	2	<b>Ours</b>	<b>71.00</b>	<b>46.10</b>
ViT-B	86.6	ARD+PRM	10	5	(Mo et al. 2022)	69.10	34.62
ViT-B	86.6	PGD	120	3	(Mao et al. 2022)	70.64	43.04
RobArch-L	104	PGD	100	3	(Peng et al. 2023)	73.44	48.94
ViT-B	86.6	PGD	300	3	(Liu et al. 2024)	74.7	49.7
ViT-B	86.6	PGD	20	3	(Wang et al. 2024)	73.4	53.0†
ViT-B	86.6	APGD	300	2	(Singh, Croce, and Hein 2023)	74.10	50.30
ViT-B	86.6	APGD	300	2	<b>Ours</b>	<b>76.32</b>	<b>54.28</b>

Therefore, we obtain a lower bound of  $I(x + \delta, z)$ . If we use CIFAR-10 ( $|F(x + \delta)| = 10$ ) and assume the predicted labels  $F(x + \delta)$  follow a uniform distribution, we can visualize the lower bound as a function of  $p_e$  as shown in Figure 2, from which we observe an obvious monotonic inverse relationship between  $I(x + \delta)$  and  $p_e$  in the range  $p_e \in [0, 0.9]$ . In fact, we can also obtain an upper bound, under the assumption that  $I(F(x + \delta), x_{re}) \approx I(x + \delta, z)$ , i.e., there is no information loss in the two Markov chains in Eq. (8).

**Proposition 3.3.** *If  $I(F(x + \delta), x_{re}) \approx I(x + \delta, z)$ , we have:*

$$I(x + \delta, z) \lesssim H(F(x_{re})) - 2p_e, \quad (15)$$

in which the notation ‘‘ $\lesssim$ ’’ refers to less than or similar to.

*Proof.* By the Hellman-Raviv inequality (Hellman and Raviv 1970; Brown 2009), we have:

$$\begin{aligned} 2p_e &\leq H(F(x + \delta)|x_{re}) \\ &= H(F(x + \delta)) - I(F(x + \delta), x_{re}) \\ &\approx H(F(x + \delta)) - I(x + \delta, z). \end{aligned} \quad (16)$$

□

Similar to the lower bound, the upper bound also indicates  $I(x + \delta, z)$  is inversely proportional to  $p_e$  as shown in Figure 2. In fact, apart from the above-mentioned lower and upper bounds, there exists an alternative and intuitive way to understand the mechanism of minimizing  $I(x + \delta, z)$ . For simplicity, let us assume the natural data  $x$  and adversarial perturbations  $\delta$  are independent<sup>3</sup>, then:

$$I(x + \delta, z) = I(x, z) + I(\delta, z). \quad (17)$$

According to (Vincent et al. 2008), minimizing the expected reconstruction error between natural sample  $x$  and

<sup>3</sup>This assumption is mild for certain scenarios, such as when considering universal or image-agnostic perturbations (Moosavi-Dezfooli et al. 2017).

corrupted input  $x + \delta$  amounts to maximizing a lower bound of the mutual information  $I(x, z)$ , even though  $z$  is a function of the corrupted input. Therefore, by minimizing  $I(x + \delta, z)$ , the network is forced to minimize  $I(\delta, z)$  (since  $I(x, z)$  is maximized). In other words, only the adversarial information about  $\delta$  has been removed from  $z$  when minimizing  $I(x + \delta, z)$ . This also explains the robustness of  $z$ .

## 4 Experiments

### 4.1 Experimental Setup

We evaluate MIMIR on three datasets: ImageNet-1K (Deng et al. 2009), Tiny-ImageNet (Le and Yang 2015), and CIFAR-10 (Krizhevsky, Hinton et al. 2009). Details of datasets are provided in Appendix A. Hyperparameters of the decoder are included in Appendix B.

**Training Setup.** We train models from scratch for all experiments. Following MAE (He et al. 2022), we do pre-training by MIMIR for 800 epochs. The number of warmup epochs is 40 for pre-training. We use AdamW (Loshchilov and Hutter 2019) as an optimizer for both pre-training and fine-tuning. The cosine decay as the learning rate scheduler is applied. At pre-training, MIMIR uses the 1-step PGD to generate adversarial examples for all three datasets. The perturbation budget is  $\epsilon = 8, \alpha = 10$ . At fine-tuning stage, we use the 10-step PGD AT with perturbation bound  $\epsilon = 8, \alpha = 2$  for CIFAR-10 and Tiny-ImageNet. For ImageNet-1K, we use 1-step PGD with random initialization for better efficiency. The perturbation bound is  $\epsilon = 4$  for ImageNet-1K. We also use a 2-step APGD with a longer fine-tuning scheduler to compare with SOTA works in Table 1. Details on training hyperparameters are provided in Appendix C.

**Evaluation Metrics.** We use **natural accuracy** and **robust accuracy** as evaluation metrics. Natural accuracy refers to the accuracy of natural and unmodified inputs. The robust accuracy measures the accuracy under the AutoAt-

Table 2: Influence of the ConvStem block. The Standard pre-trained weights refer to pre-trained weights from `timm`. The configurations are `deit_small_patch16_224` and `vit_base_patch16_224_augreg_in1k`. The weights are fine-tuned 300 epochs by 2-step APGD. †The result on ViT-S is taken from (Singh, Croce, and Hein 2023).

Architecture	Pre-trained weights	Natural	Robust
ViT-S+ConvStem	Standard	72.56	48.08†
	MIMIR	<b>72.72</b>	<b>48.44</b>
ViT-B+ConvStem	Standard	75.26	52.70
	MIMIR	<b>76.72</b>	<b>54.04</b>

tack (Francesco and Hein 2020). AutoAttack is an ensemble of diverse parameter-free attacks, including white-box and black-box attacks. In our experiments, we use standard version of AutoAttack that contains four attacks, including APGD-ce (Francesco and Hein 2020), APGD-t (Francesco and Hein 2020), FAB-t (Croce and Hein 2020), and Square (Andriushchenko et al. 2020). The perturbation budgets are  $\epsilon = 8$  for CIFAR-10 and Tiny-ImageNet,  $\epsilon = 4$  for ImageNet-1K.

## 4.2 Experimental Results

**Comparison with SOTA Works.** Table 1 compares MIMIR with previous works concerning adversarial robustness on ImageNet-1K ( $l_\infty, \epsilon = 4/255$ ). We report the number of parameters, training epochs, steps in the inner maximization of AT, and clean and robust accuracy. The robust accuracy is evaluated by AutoAttack on the RobustBench validation set (5000 images). We divide the models into two groups: *small* ( $\approx 22$ M) and *large* ( $\approx 86$ M) models. In addition, (Singh, Croce, and Hein 2023) shows that the Convolutional stem (ConvStem) improves the robustness of ViTs. We also include an evaluation of ViTs+ConvStem in Table 2. ConvStem (Xiao et al. 2021) refers to replacing the patch embedding in ViTs with a convolutional block. MIMIR outperforms all SOTA works.

**Ablation Study.** Table 3 provides an ablation study to verify the design choices of MIMIR. The ablation uses 100 epochs of 1-step PGD (PGD<sub>1</sub>) AT as the baseline. Then, we apply end-to-end clean ImageNet-1K pre-training (weights available in `timm` library) as initialization of AT. After that, we replace the clean pre-training with MAE, adv MAE, and MIMIR step by step. The adv MAE refers to using adversarial examples but not using the MI  $I(x+\delta, z)$  in loss. The pre-training scheduler is 800 epochs. We also use stronger adversarial fine-tuning for better performance, including 2-step PGD (PGD<sub>2</sub>), APGD (APGD<sub>2</sub>) FT, and a longer fine-tuning scheduler (300 epochs). Please note that a longer training scheduler does not guarantee better results (Mo et al. 2022). Our results indicate that MIMIR outperforms baselines and can be further improved under the long training scheduler.

In addition, MIMIR is also efficient and increases less than 5% of time consumption on ImageNet-1K compared to MAE, which is shown in Table 12 in the Appendix E.

**MI Measure.** In Section 3.4, we provide lower and upper

Table 3: Ablation of pre-training (PT) and fine-tuning (FT) methods on ImageNet-1K. (†: catastrophic overfitting (Wong, Rice, and Kolter 2020) due to 1-step AT at fine-tuning, which can be fixed by 2-step AT. The fixed natural and robust accuracy are 69.96 and 36.90, respectively.)

Architecture	Training Recipe	Natural	Robust
ViT-S	PGD <sub>1</sub> FT w/o PT	66.02	31.40
	clean PT + PGD <sub>1</sub> FT	67.04	33.70
	MAE PT + PGD <sub>1</sub> FT	69.98	35.64
	adv MAE PT + PGD <sub>1</sub> FT	68.24	19.32†
	MIMIR PT + PGD <sub>1</sub> FT	71.02	37.22
	MIMIR PT + PGD <sub>2</sub> FT	70.78	38.16
	MIMIR PT + APGD <sub>2</sub> FT	68.78	42.86
	100 $\rightarrow$ 300 epochs FT	71.00	46.10

Table 4: Comparison between HSIC (Gretton et al. 2005) and  $I_\alpha$  (Yu, Yu, and Príncipe 2021) using ViT-T on CIFAR-10. Models are pre-trained 800 epochs and adversarially fine-tuned with 10-step PGD for 50 epochs.

Pre-train	$\lambda$	Estimator	Natural	PGD
MIMIR	0.001	HSIC	69.63	43.17
MIMIR	0.001	$I_\alpha$	75.00	46.11
MIMIR	1e-05	HSIC	<b>76.30</b>	<b>47.60</b>
MIMIR	1e-05	$I_\alpha$	75.53	46.75
MIMIR	1e-06	HSIC	74.90	46.19
MIMIR	1e-06	$I_\alpha$	74.60	45.66

bound (Eq. (11)) of  $I(x+\delta, z)$ . According to the two bounds,  $I(x+\delta, z)$  is supposed to decrease while the autoencoder learns to reconstruct the natural image  $x$ . This motivates us to directly embed  $I(x+\delta, z)$  as a minimizing learning objective. In this paper, we use  $I_\alpha$  (Yu, Yu, and Príncipe 2021) and HSIC (Ma, Lewis, and Kleijn 2020) as estimators (detailed definitions in Appendix F). Table 4 demonstrates the performance of different values of  $\lambda$ . According to the results, we use HSIC with  $\lambda = 1e-05$  for all other experiments.

**1-step is better than 10-step of AT in pre-training.** We also show that MIMIR outperforms original MAE (He et al. 2022) and adv MAE with different PGD steps (to generate adversarial examples for training). MAE in Table 5 refers to using the original MAE for pre-training and then fine-tuning with 10-step PGD. The adv MAE refers to using adversarial examples without the MI  $I(x+\delta, z)$  in loss. The adv MAE (10-steps) refers to using the 10-step PGD algorithm ( $\epsilon = 8, \alpha = 2$ ) to generate adversarial examples at pre-training. The adv MAE provides higher accuracy than MAE, which supports our statement that using adversarial examples in Masked Image Modeling creates a more difficult reconstruction task. This more difficult task further improves the performance of downstream models (See also Table 7). We use the default learning rate (i.e.,  $5.0e-4$ ) of MAE, so there is a performance drop in experiments in Table 5 and 4 since AT prefers larger learning rates on CIFAR-10 as shown in Table 11 in the Appendix.

**Stability.** Due to the high computation cost, we cannot re-

Table 5: Comparison between different pre-training settings. All models are pre-trained for 800 epochs and then fine-tuned with 10-step PGD for 50 epochs using ViT-T on CIFAR-10.

Pre-train	$\lambda$	Estimator	Natural	PGD
MAE	0.0	-	69.02	42.31
adv MAE (1-step)	0.0	-	74.69	46.28
adv MAE (10-step)	0.0	-	73.96	45.77
MIMIR	1e-05	HSIC	<b>76.30</b>	<b>47.60</b>

Table 6: Adversarial accuracy by adaptive attacks. The models are pre-trained 800 epochs by MIMIR and fine-tuned 100 epochs by PGD AT.

Dataset	Model	PGD <sub>20</sub>	PGD-MI <sub>100</sub>	PGD-fea <sub>100</sub>
CIFAR-10	ConViT-S	56.35	56.16	78.52
	ViT-S	56.63	56.31	78.41
	ViT-B	58.14	57.85	80.49
Tiny-ImageNet	ConViT-S	26.39	26.29	58.50
	ViT-S	26.37	26.18	57.36
	ViT-B	25.41	25.05	58.90
ImageNet-1K	ConViT-S	53.86	53.84	72.10
	ViT-S	54.56	54.55	72.27
	ViT-B	55.41	55.36	73.51

port standard deviation for all experiments. To show that our method MIMIR has low variances, we train ViT-S on CIFAR-10 three times with different random seeds, running pre-training 400 epochs and fine-tuning 50 epochs. The natural accuracy is  $86.07 \pm 0.16$  %. The adversarial accuracy under PGD<sub>20</sub> ( $l_\infty$ ,  $\epsilon = 8/255$ ) is  $47.24 \pm 0.12$  %.

**Adaptive Attacks.** We evaluate MIMIR against adaptive adversaries following common practices (Tramer et al. 2020). We provide two adaptive attacks specifically designed against MIMIR. First, we introduce the PGD Mutual Information attack (PGD-MI), which utilizes the MI  $I(x + \delta, z)$  to generate adversarial examples, as  $I(x + \delta, z)$  is used in MIMIR pre-training as a penalty in the loss. PGD-MI attacks the model by directly increasing the MI  $I(x + \delta, z)$ . Specifically, we add the MI loss into the PGD algorithm:

$$\max_{\delta \in S} \mathcal{L}_{CE}(x_i + \delta, y_i) + \lambda I(x + \delta, z). \quad (18)$$

where the value of  $\lambda$  in MIMIR pre-training is available to adversaries.

Second, we introduce a PGD feature attack (PGD-fea) that directly attacks the feature extracted by ViT backbones following (Sabour et al. 2016). In particular, we attack the feature extractor from the backbones after the adversarial fine-tuning. The PGD-fea attack increases the Euclidean distance between features extracted from natural and adversarial examples. We implement it using the PGD algorithm:

$$\max_{\delta \in S} \mathcal{L}_{mse}(f_e(x), f_e(x + \delta)). \quad (19)$$

Both PGD-MI and PGD-fea are optimized for 100 steps to make sure the attacking algorithm converges. The perturbation budget is the same as the previous evaluation, i.e.,  $\epsilon =$

Table 7: Natural accuracy of MAE and MIMIR (800 epochs pre-training for both) that are fine-tuned on natural images.

Architecture	Pre-train	CIFAR-10	Tiny	ImageNet
ViT-B	MAE	96.79	73.38	82.92
	MIMIR	<b>96.91</b>	<b>75.43</b>	<b>83.20</b>
ConViT-S	MAE	94.95	69.03	78.37
	MIMIR	<b>95.38</b>	<b>70.40</b>	<b>79.21</b>
ViT-S	MAE	95.95	70.00	77.45
	MIMIR	95.95	<b>71.14</b>	<b>78.69</b>

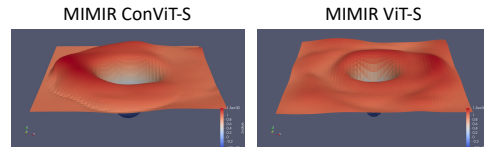


Figure 3: The loss landscapes of MIMIR pre-trained models.

$8/255$  for CIFAR-10 and Tiny-ImageNet, and  $\epsilon = 4/255$  for ImageNet-1K. Table 6 demonstrates the adaptive evaluation results for PGD-MI and PGD-fea attacks, showing that MIMIR is robust against adaptive attacks on benchmark datasets.

**Visualization of the Loss Landscape.** To show that the robustness of MIMIR-trained models does not stem from gradient masking, we plot the loss landscape (Li et al. 2018) in Figure 3. The loss landscape is the visualization of the loss function as parameters change. The basic idea is to plot the loss around the optimal parameters. The landscapes of all models are smooth, i.e., the gradient at a certain point is clear and can also be easily estimated by local average gradients, which means the gradient is masked.

**Fine-tuning with Natural Images.** In Table 7, we show the results of MIMIR and the original MAE (He et al. 2022) with the same hyperparameter. We fine-tune 50 epochs for CIFAR-10 and Tiny-ImageNet, 100 epochs for ImageNet-1K. Surprisingly, MIMIR outperforms MAE when fine-tuning with natural data. We leave further exploration of this finding to future work.

## 5 Conclusions and Future Work

This paper provides a novel theoretical MI analysis on ViT adversarial training, showing that MI between the adversarial example and its latent representation in ViT-based autoencoders, i.e.,  $I(x + \delta, z)$ , should be constrained by utilizing the MI bounds. Based on this finding, we propose MIMIR as a theoretically grounded pre-training method to improve adversarial robustness for ViTs. MIMIR uses adversarial examples as inputs and natural data as the reconstruction target. In this way, the information from the adversarial perturbations is decreased by the bottleneck, while the information from natural data is preserved while reconstructing the target. Our experimental results show that MIMIR substantially improves adversarial robustness compared to recent related works on various benchmark datasets.

## References

- Alemi, A. A.; Fischer, I.; Dillon, J. V.; and Murphy, K. 2017. Deep Variational Information Bottleneck. In *ICLR*.
- Andriushchenko, M.; Croce, F.; Flammarion, N.; and Hein, M. 2020. Square Attack: A Query-Efficient Black-Box Adversarial Attack via Random Search. In *ECCV*.
- Athalye, A.; Carlini, N.; and Wagner, D. 2018. Obfuscated Gradients Give a False Sense of Security: Circumventing Defenses to Adversarial Examples. In *ICML*.
- Bai, Y.; Mei, J.; Yuille, A. L.; and Xie, C. 2021. Are Transformers more robust than CNNs? In *NeurIPS*.
- Bao, H.; Dong, L.; Piao, S.; and Wei, F. 2022. BEiT: BERT Pre-Training of Image Transformers. In *ICLR*.
- Beaudry, N. J.; and Renner, R. 2011. An intuitive proof of the data processing inequality. *arXiv preprint arXiv:1107.0740*.
- Biggio, B.; Corona, I.; Maiorca, D.; Nelson, B.; Šrndić, N.; Laskov, P.; Giacinto, G.; and Roli, F. 2013. Evasion Attacks against Machine Learning at Test Time. In *ECML PKDD*.
- Brown, G. 2009. An information theoretic perspective on multiple classifier systems. In *International Workshop on Multiple Classifier Systems*.
- Croce, F.; and Hein, M. 2020. Minimally distorted Adversarial Examples with a Fast Adaptive Boundary Attack. In *ICML*.
- Cubuk, E. D.; Zoph, B.; Shlens, J.; and Le, Q. 2020. RandAugment: Practical Automated Data Augmentation with a Reduced Search Space. In *NeurIPS*.
- Dalvi, N.; Domingos, P.; Mausam, Sanghai, S.; and Verma, D. 2004. Adversarial Classification. In *KDD*.
- D’Ascoli, S.; Touvron, H.; Leavitt, M. L.; Morcos, A. S.; Biroli, G.; and Sagun, L. 2021. ConViT: Improving Vision Transformers with Soft Convolutional Inductive Biases. In *ICML*.
- Debenedetti, E.; Sehwan, V.; and Mittal, P. 2023. A Light Recipe to Train Robust Vision Transformers. In *SatML*.
- Deng, J.; Dong, W.; Socher, R.; Li, L.-J.; Li, K.; and Fei-Fei, L. 2009. ImageNet: A large-scale hierarchical image database. In *2009 IEEE Conference on Computer Vision and Pattern Recognition*.
- Dosovitskiy, A.; Beyer, L.; Kolesnikov, A.; Weissenborn, D.; Zhai, X.; Unterthiner, T.; Dehghani, M.; Minderer, M.; Heigold, G.; Gelly, S.; Uszkoreit, J.; and Housley, N. 2021. An Image is Worth 16x16 Words: Transformers for Image Recognition at Scale. In *ICLR*.
- Fano, R. M. 1949. *The transmission of information*, volume 65. Massachusetts Institute of Technology, Research Laboratory of Electronics . . . .
- Francesco, C.; and Hein, M. 2020. Reliable evaluation of adversarial robustness with an ensemble of diverse parameter-free attacks. In *ICML*.
- Gretton, A.; Bousquet, O.; Smola, A.; and Schölkopf, B. 2005. Measuring Statistical Dependence with Hilbert-Schmidt Norms. In *Algorithmic Learning Theory*.
- He, K.; Chen, X.; Xie, S.; Li, Y.; Dollár, P.; and Girshick, R. 2022. Masked Autoencoders Are Scalable Vision Learners. In *CVPR*.
- Hellman, M.; and Raviv, J. 1970. Probability of error, equivocation, and the Chernoff bound. *IEEE Transactions on Information Theory*, 16(4): 368–372.
- Krizhevsky, A.; Hinton, G.; et al. 2009. Learning multiple layers of features from tiny images.
- Le, Y.; and Yang, X. 2015. Tiny imagenet visual recognition challenge. *CS 231N*, 7(7): 3.
- Li, H.; Xu, Z.; Taylor, G.; Studer, C.; and Goldstein, T. 2018. Visualizing the Loss Landscape of Neural Nets. In *NeurIPS*.
- Liu, C.; Dong, Y.; Xiang, W.; Yang, X.; Su, H.; Zhu, J.; Chen, Y.; He, Y.; Xue, H.; and Zheng, S. 2024. A comprehensive study on robustness of image classification models: Benchmarking and rethinking. *IJCV*.
- Loshchilov, I.; and Hutter, F. 2019. Decoupled Weight Decay Regularization. In *ICLR*.
- Ma, W.-D. K.; Lewis, J. P.; and Kleijn, W. B. 2020. The HSIC Bottleneck: Deep Learning without Back-Propagation. In *AAAI*.
- Madry, A.; Makelov, A.; Schmidt, L.; Tsipras, D.; and Vladu, A. 2018. Towards Deep Learning Models Resistant to Adversarial Attacks. In *ICLR*.
- Mao, X.; Chen, Y.; Li, X.; Qi, G.; Duan, R.; Zhang, R.; and Xue, H. 2022. EasyRobust: A Comprehensive and Easy-to-use Toolkit for Robust Computer Vision. <https://github.com/alibaba/easyrobust>.
- Mo, Y.; Wu, D.; Wang, Y.; Guo, Y.; and Wang, Y. 2022. When Adversarial Training Meets Vision Transformers: Recipes from Training to Architecture. In *NeurIPS*.
- Moosavi-Dezfooli, S.-M.; Fawzi, A.; Fawzi, O.; and Frossard, P. 2017. Universal Adversarial Perturbations. In *CVPR*.
- Ocal, O.; Elibol, O. H.; Keskin, G.; Stephenson, C.; Thomas, A.; and Ramchandran, K. 2019. Adversarially Trained Autoencoders for Parallel-data-free Voice Conversion. In *ICASSP*.
- Peng, S.; Xu, W.; Cornelius, C.; Li, K.; Duggal, R.; Chau, D. H.; and Martin, J. 2023. RobArch: Designing Robust Architectures against Adversarial Attacks. *arXiv:2301.03110*.
- Radford, A.; Kim, J. W.; Hallacy, C.; Ramesh, A.; Goh, G.; Agarwal, S.; Sastry, G.; Askell, A.; Mishkin, P.; Clark, J.; Krueger, G.; and Sutskever, I. 2021. Learning Transferable Visual Models From Natural Language Supervision. In *Proceedings of the 38th International Conference on Machine Learning*.
- Sabour, S.; Cao, Y.; Faghri, F.; and Fleet, D. J. 2016. Adversarial Manipulation of Deep Representations. In *ICLR*.
- Sanchez Giraldo, L. G.; Rao, M.; and Principe, J. C. 2015. Measures of Entropy From Data Using Infinitely Divisible Kernels. *IEEE Transactions on Information Theory*, 61(1): 535–548.
- Shwartz-Ziv, R.; and Tishby, N. 2017. Opening the Black Box of Deep Neural Networks via Information. *CoRR*, abs/1703.00810.



- Singh, N. D.; Croce, F.; and Hein, M. 2023. Revisiting Adversarial Training for ImageNet: Architectures, Training and Generalization across Threat Models. In *NeurIPS*.
- Szegedy, C.; Zaremba, W.; Sutskever, I.; Bruna, J.; Erhan, D.; Goodfellow, I.; and Fergus, R. 2014. Intriguing properties of neural networks. In *ICLR*.
- Tishby, N.; Pereira, F. C. N.; and Bialek, W. 2000. The information bottleneck method. *CoRR*, physics/0004057.
- Tishby, N.; and Zaslavsky, N. 2015. Deep learning and the information bottleneck principle. In *2015 IEEE Information Theory Workshop (ITW)*.
- Tramer, F.; Carlini, N.; Brendel, W.; and Madry, A. 2020. On Adaptive Attacks to Adversarial Example Defenses. In *NeurIPS*.
- Vincent, P.; Larochelle, H.; Bengio, Y.; and Manzagol, P.-A. 2008. Extracting and composing robust features with denoising autoencoders. In *ICML*.
- Vincent, P.; Larochelle, H.; Lajoie, I.; Bengio, Y.; Manzagol, P.-A.; and Bottou, L. 2010. Stacked denoising autoencoders: Learning useful representations in a deep network with a local denoising criterion. *Journal of machine learning research*, 11(110): 3371–3408.
- Wang, H.; Song, K.; Fan, J.; Wang, Y.; Xie, J.; and Zhang, Z. 2023. Hard Patches Mining for Masked Image Modeling. In *CVPR*.
- Wang, Z.; Jian, T.; Masoomi, A.; Ioannidis, S.; and Dy, J. 2021. Revisiting Hilbert-Schmidt Information Bottleneck for Adversarial Robustness. In *NeurIPS*.
- Wang, Z.; Li, X.; Zhu, H.; and Xie, C. 2024. Revisiting Adversarial Training at Scale. *CVPR*.
- Wei, C.; Fan, H.; Xie, S.; Wu, C.-Y.; Yuille, A.; and Feichtenhofer, C. 2022. Masked Feature Prediction for Self-Supervised Visual Pre-Training. In *CVPR*.
- Wong, E.; Rice, L.; and Kolter, J. Z. 2020. Fast is better than free: Revisiting adversarial training. In *ICLR*.
- Wu, B.; Gu, J.; Li, Z.; Cai, D.; He, X.; and Liu, W. 2022. Towards Efficient Adversarial Training on Vision Transformers. In *ECCV*.
- Xiao, T.; Singh, M.; Mintun, E.; Darrell, T.; Dollar, P.; and Girshick, R. 2021. Early Convolutions Help Transformers See Better. In *NeurIPS*.
- Xie, Z.; Zhang, Z.; Cao, Y.; Lin, Y.; Bao, J.; Yao, Z.; Dai, Q.; and Hu, H. 2022. SimMIM: A Simple Framework for Masked Image Modeling. In *CVPR*.
- Xu, X.; Perin, G.; and Pícek, S. 2023. IB-RAR: Information Bottleneck as Regularizer for Adversarial Robustness. In *DSN-W*.
- Yu, S.; Giraldo, L. G. S.; Jenssen, R.; and Principe, J. C. 2019. Multivariate Extension of Matrix-Based Renyi’s alpha-Order Entropy Functional. *IEEE transactions on pattern analysis and machine intelligence*, 42(11): 2960–2966.
- Yu, X.; Yu, S.; and Principe, J. C. 2021. Deep Deterministic Information Bottleneck with Matrix-Based Entropy Functional. In *ICASSP*.
- Yun, S.; Han, D.; Oh, S. J.; Chun, S.; Choe, J.; and Yoo, Y. 2019. CutMix: Regularization Strategy to Train Strong Classifiers With Localizable Features. In *ICCV*.
- Zhang, H.; Cissé, M.; Dauphin, Y. N.; and Lopez-Paz, D. 2018. mixup: Beyond Empirical Risk Minimization. In *ICLR*.

## A Datasets

We use three commonly used datasets to evaluate MIMIR: CIFAR-10 (Krizhevsky, Hinton et al. 2009), Tiny-ImageNet (Le and Yang 2015), and ImageNet-1K (Deng et al. 2009). CIFAR-10 (Krizhevsky, Hinton et al. 2009) comprises 50,000 images with size  $3 \times 32 \times 32$  in 10 classes. ImageNet-1K (Deng et al. 2009) is the most commonly used dataset for the evaluation of ViTs and its variants, which is composed of more than 1.2 million high-resolution images in 1,000 classes. In our experiments, images from ImageNet-1K are resized to  $3 \times 224 \times 224$ . For completeness, we also include Tiny-ImageNet (Le and Yang 2015) as a medium size dataset between CIFAR-10 (Krizhevsky, Hinton et al. 2009) and ImageNet-1K (Deng et al. 2009). Tiny-ImageNet (Le and Yang 2015) contains 100,000 images with size  $3 \times 64 \times 64$  in 200 classes.

## B Decoder Hyperparameters

We use transformer blocks but fewer layers as the backbone of the decoder. For CIFAR-10, we use the patch size of 2, 4 for Tiny-ImageNet, and 16 for ImageNet-1K. Table 8 shows the hyperparameters of decoder architectures. For different ViT architectures, we use the transformer blocks of the respective architectures to build the encoder.

Table 8: Model architectures of the encoder and decoder.

Model	Layers	Hidden size	MLP ratio	Heads
ViT-T (encoder)	12	192	4	3
decoder	2	128	4	16

## C Details of Training Hyperparameters

In Tables 9 and 10, we provide the default hyperparameters used in our experiments. In addition, we use different patch sizes for different datasets: patch size 2 for CIFAR-10, 4 for Tiny-ImageNet, and 16 for ImageNet-1K. Using smaller patch sizes increases the time consumption when calculating self-attention, but MIMIR pre-training discards 75% patches, making it still efficient.

**Hardware.** Experiments are performed on a single machine with 4 RTX A6000 (48GB) and 4 RTX A5000 (24GB) GPUs, CUDA 12.0.

Table 9: Pre-training hyperparameters.

Config	Value
optimizer	AdamW
base learning rate	$1.5e-4$
weight decay	0.05
optimizer momentum	$\beta_1 = 0.9, \beta_2 = 0.95$
batch size	512(CIFAR-10, Tiny), 2,048 (ImageNet-1K)
learning rate schedule	cosine decay
warmup epochs	40
training epochs	800
augmentation	RandomResizedCrop, RandomHorizontalFlip

Table 10: Fine-tuning hyperparameters.

Config	Value
optimizer	AdamW
base learning rate	$0.5e-2$ (CIFAR-10), $1e-3$ (ImageNet-1K, Tiny)
weight decay	0.05
optimizer momentum	$\beta_1 = 0.9, \beta_2 = 0.999$
layer-wise lr decay	0.65, 1.0
batch size	128 (CIFAR-10), 256 (Tiny), 1,024 (ImageNet-1K)
learning rate schedule	cosine decay
warmup epochs	10, 20
training epochs	100, 300
augmentation	RandomResizedCrop, RandomHorizontalFlip
drop path	0.1

Table 11: Different learning rates. Fine-tuned for 50 epochs.

Dataset	Models	LR	Natural	PGD <sub>10</sub>
CIFAR-10	ViT-T	$5.0e-4$	76.30	47.60
		$1.0e-3$	80.69	49.56
		$1.0e-2$	85.62	48.78
		$5.0e-2$	85.12	50.30
		$1.0e-1$	84.51	50.40

## D Training Epochs Evaluation Study

**Pre-training epoch.** Our experiments so far are based on 800-epoch pre-training. In Figure 4, we show the influence of different numbers of epochs. We use ViT-T and ViT-S as the models for CIFAR-10, ViT-S, and ViT-B for Tiny-ImageNet. We fine-tune each model 50 epochs after MIMIR pre-training. Both adversarial and natural accuracy are improved with a longer training schedule. On CIFAR-10, the improvement of ViT-T is more significant than that of ViT-S. On Tiny-ImageNet, the increase is more obvious. Therefore, a longer pre-training schedule obviously increases performance.

**Fine-tuning epoch.** To show that the performance of the final model is largely attributed to MIMIR pre-training, we do a very short fine-tuning for pre-trained models. This is to train the randomly initialized classification layer since we do not have the classification layer at pre-training. Therefore, we evaluate the pre-training performance. In Figure 5, we show that MIMIR pre-training plus 5 or 10 epochs of fine-tuning is enough to achieve similar performance compared to 100-epoch fine-tuning.

## E Efficiency

Table 12 provides the time consumption and memory usage of MIMIR and adversarial training at fine-tuning. The time consumption and memory usage are evaluated on 4 A6000 GPUs. Compared to 10-step PGD and FastAT, MIMIR shows much less time consumption. At pre-training, MIMIR shows slightly higher time consumption than MAE, resulting from generating adversarial examples and calculating MI between  $x + \delta$  and  $z$ . Still, as we use a one-step algorithm, generating adversarial examples does not cost too

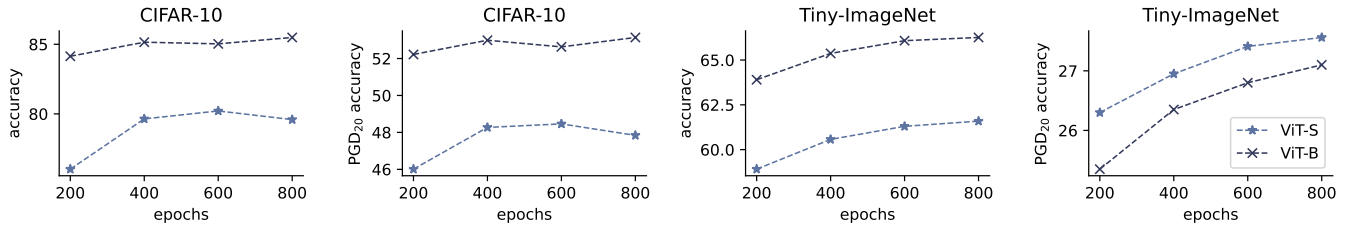


Figure 4: Natural and adversarial accuracy of ViT-S and ViT-B that are fine-tuned with different numbers of pre-train epochs under a 20-step PGD attack.

Table 12: The average time consumption of a single epoch on 4 GPUs. The “mem.” refers to GPU memory usage.

Architecture	#Parames (M)	Method	CIFAR-10		Tiny-ImageNet		ImageNet-1K	
			time[S]	mem.[GB]	time[S]	mem.[GB]	time[S]	mem.[GB]
ViT-S	21.34	PGD <sub>10</sub> AT	149.3	2.54×4	306.0	3.99×4	2251.7	12.5×4
		FastAT	43.3	2.54×4	67.7	4.03×4	555.5	10.4×4
		MAE	16.1	3.24×4	33.0	3.27×4	269.6	11.1×4
		MIMIR	18.4	3.12×4	40.0	3.18×4	275.5	11.1×4
ViT-B	85.27	PGD <sub>10</sub> AT	361.2	5.39×4	1022.2	8.30×4	5416.7	22.1×4
		FastAT	122.8	5.36×4	180.2	8.34×4	1361.3	19.8×4
		MAE	53.0	5.95×4	106.5	5.95×4	490.9	17.0×4
		MIMIR	59.0	6.08×4	122.0	6.11×4	509.9	17.0×4
ConViT-S	27.05	PGD <sub>10</sub> AT	442.5	6.64×4	897.0	12.19×4	6626.5	32.5×4
		FastAT	106.5	5.86×4	183.2	10.62×4	1431.2	26.4×4
		MAE	33.0	10.6×4	67.5	10.61×4	609.7	27.5×4
		MIMIR	45.0	10.4×4	90.0	10.54×4	611.1	28.3×4

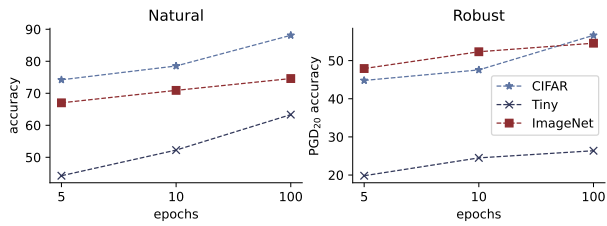


Figure 5: Natural and adversarial accuracy of ViT-S adversarially fine-tuned for 5 or 10 epochs on CIFAR-10, Tiny-ImageNet, and ImageNet-1K.

much time. We also consider using a 10-step PGD at pre-training. Table 5 shows that using a one-step algorithm with larger  $\alpha = 10$  provides better performance. In addition, pre-training with MIMIR also costs less memory. Note in Table 12 that the batch size for MIMIR pre-training is much larger than the batch size for adversarial fine-tuning. In Table 12, a single epoch of MIMIR costs about  $\frac{1}{8}$  time consumption compared to 10-step PGD adversarial training, and about  $\frac{1}{2}$  compared to 1-step fast adversarial training (Wong, Rice, and Kolter 2020). Therefore, MIMIR is more promising regarding training costs when conducting adversarial training.

## F Mutual Information and HSIC

MI measures the mutual dependence between two random variables,  $X$  and  $Y$ . It can be decomposed as:

$$\begin{aligned}
 I(X, Y) &= H(X) - H(X|Y), \\
 &= H(Y) - H(Y|X), \\
 &= H(X) + H(Y) - H(X, Y),
 \end{aligned}
 \tag{20}$$

where  $H(X)$  and  $H(Y)$  are the information entropies,  $H(X|Y)$  and  $H(Y|X)$  are the conditional entropies, and  $H(X, Y)$  is the joint entropy of  $X$  and  $Y$ .

Unfortunately, estimating MI in high-dimensional space is a difficult task since it may involve a precise estimation of the underlying data distribution  $P_{(X,Y)}$  or  $P_{(X)}$  and  $P_{(Y)}$ . To address this issue, the deterministic information bottleneck (DIB) (Yu, Yu, and Príncipe 2021) uses the recently proposed matrix-based Rényi’s  $\alpha$ -entropy functional  $I_\alpha$  (Sanchez Giraldo, Rao, and Principe 2015; Yu et al. 2019), which suggests similar quantities to  $I(X, Y)$  in terms of the normalized eigenspectrum of the hermitian matrix of the projected data in the reproducing kernel Hilbert space (RKHS), but avoids density estimation.

Specifically, given  $N$  pairs of samples  $(x_i, y_i)_{i=1}^N$  (in our setup,  $N$  refers to the mini-batch size), we can obtain two Gram (or kernel) matrices  $K_x$  and  $K_y$ , for variables  $X$  and  $Y$ , respectively, with  $(K_x)_{i,j} = \kappa_x(x_i, x_j)$ ,  $(K_y)_{i,j} = \kappa_y(y_i, y_j)$ , in which  $\kappa_x$  and  $\kappa_y$  are corresponding kernel functions. The information entropy of  $X$  can be

expressed as:

$$H_\alpha(X) = \frac{1}{1-\alpha} \log_2 \left( \text{tr}(\tilde{K}_x^\alpha) \right) = \frac{1}{1-\alpha} \log_2 \left( \sum_{i=1}^N \lambda_i(\tilde{K}_x)^\alpha \right), \quad (21)$$

where  $\tilde{K}$  is the normalized version of  $K$ , i.e.,  $\tilde{K} = K/\text{tr}(K)$ , and  $\lambda_i(\tilde{K})$  denotes the  $i$ -th eigenvalue of  $\tilde{K}$ .

Further, the joint entropy for  $X$  and  $Y$  can be expressed as:

$$H_\alpha(X, Y) = H_\alpha \left( \frac{K_x \circ K_y}{\text{tr}(K_x \circ K_y)} \right), \quad (22)$$

where  $K_x \circ K_y$  denotes the Hadamard product between the matrices  $K_x$  and  $K_y$ .

Given Eqs. (21) and (22), the matrix-based Rényi's  $\alpha$ -order mutual information  $I_\alpha(X; Y)$  in analogy of Shannon's MI is given by:

$$I_\alpha(X; Y) = H_\alpha(X) + H_\alpha(Y) - H_\alpha(X, Y). \quad (23)$$

Throughout this paper, we use the radial basis function (RBF) kernel  $\kappa(x_i, x_j) = \exp(-\frac{\|x_i - x_j\|^2}{2\sigma^2})$  with kernel width  $\sigma$  to obtain the Gram matrices.

The Hilbert–Schmidt Independence Criterion (HSIC) (Gretton et al. 2005) is also a kernel-based dependence measure and is usually used as a surrogate of MI. Formally, the HSIC is defined as the squared norm of the cross-covariance operator  $\|C_{XY}\|^2$ :

$$\begin{aligned} \text{HSIC}_{P_{X,Y}}(X, Y) &= \|C_{XY}\|^2 \\ &= \mathbb{E}_{x y x' y'} [\kappa_x(x, x') \kappa_{y'}(y, y')] \\ &\quad + \mathbb{E}_{x x'} [\kappa_x(x, x')] \mathbb{E}_{y y'} [\kappa_y(y, y')] \\ &\quad - 2\mathbb{E}_{x y} [\mathbb{E}_{x'} [\kappa_x(x, x')] \mathbb{E}_{y'} [\kappa_y(y, y')]], \end{aligned} \quad (24)$$

where  $\kappa_x$  and  $\kappa_y$  are kernel functions,  $\mathbb{E}$  is the expectation,  $x'$  and  $y'$  are independent copies of  $x$  and  $y$ , respectively.

Given  $N$  pairs of samples  $(x_i, y_i)_{i=1}^N$ , the empirical estimator of HSIC is given by:

$$\widehat{\text{HSIC}}_{P_{X,Y}}(X, Y) = \frac{1}{N^2} \text{tr}(K_x H H_y H), \quad (25)$$

in which  $(K_x)_{i,j} = \kappa_x(x_i, x_j)$ ,  $(K_y)_{i,j} = \kappa_y(y_i, y_j)$ , and  $H = I - \frac{1}{N} \mathbf{1}\mathbf{1}^T$  is the centering matrix.